Acta Oncologica Vol. 32, Nos. 7/8, pp. 763–769, 1993

IMAGE SUBTRACTION ANALYSIS WITH TECHNETIUM-99M LABELED MONOCLONAL ANTIBODY AND COLLOID FOR EVALUATION OF LIVER LESIONS

Phantom measurements and patient studies

KALEVI J. A. KAIREMO, AARO J. KIURU and JORMA J. HEIKKONEN

The ideal radiolabeled monoclonal antibodies (MoAbs) against cancer antigens are taken up by liver metastases; the background activity of normal liver, however, causes problems for delineation and detectability. In order to study these phenomena, a liver phantom containing hot and cold lesions of different sizes (diameters 5–32 mm) was constructed. It was placed into an elliptic cylindrical container representing a cross section of the abdomen. The specific activities in hot lesions varied from 1.85 to 14.8 MBq/ml, whereas liver phantom and cylinder activities were kept constant during different measurements. Lesions of size 1.3 cm^3 could be detected without any subtractions, if the signal to background ratio was larger than 1.2. Lesions larger than 5 mm in diameter could also be detected using subtraction, which gave additional information by a factor 2–9, when the lesion sizes varied from 0.3 to 5.3 cm^3 and when the specific activity in the lesions was at least twice as high as in adjacent liver. This subtraction technique was applied in 32 breast and lung cancer patients after injecting about 1 000 MBq ^{99m}Tc-labeled anti-CEA MoAb; 24 h after the antibody injection 75 MBq ^{99m}Tc-phytate was injected. The phytate + residual MoAb image was subtracted from the original antibody image. Thirteen patients had liver metastases verified by (CT, US), but only four patients had clearly observable abnormal liver uptakes in planar MoAb images. In 9 cases, additional information concerning liver metastases was obtained by subtraction technique. To judge by our phantom measurements the enhanced detectability was not an artefact.

Radiolabeled antibodies have been used for years for detection of malignant liver tumors (1, 2). The low specificity and high activity in the normal liver tissue, however, can cause problems for delineation and detectability of the lesions. High liver activities (up to 15–20% of the injected antibody dose) cannot be avoided. It can be reduced by RES blockade, cold antibody injection, internal labeling of antibodies, anti-antibody injections, separate label and antibody injections, ligand modification, and proper radionuclide and fragment selection (3–7).

Detection of liver metastases is very important for staging but the high uptake in normal liver tissue is a disturbing factor. Therefore subtraction procedures have been introduced and might be helpful for staging purposes. In the literature several subtraction methods have been described, including statistical analysis of suspected areas (8), spatial probability mapping (9), dynamic graded subtraction (10), maximum entropy deconvolution analysis (11), variable thresholds for subtraction (12), and geometrical and gray scale statistical analysis (13). Subtraction artefacts are considerably decreased when radionuclides with

Received 2 February 1993.
Accepted 22 October 1993.
From the Departments of Clinical Chemistry (K. Kairemo), and Radiotherapy and Oncology (J. Heikkonen), Helsinki University Central Hospital, Helsinki, and the Department of Oncology and Radiotherapy, University Hospital, Turku (A. Kiuru), Finland.
Correspondence to: Dr K. Kairemo, Department of Clinical Chemistry, Nuclear Medicine Division, Helsinki University Central Hospital, Haartmaninkatu 4, SF-00290 Helsinki, Finland.
Presented at the 3rd Scandinavian Symposium on Monoclonal Antibodies in Diagnosis and Therapy of Cancer, October 30–31, 1992, Helsinki, Finland.

similar photon energies are used (14) and dual-tracer studies are controlled with experimental models (15).

Double tracer subtraction studies have been performed with $^{131}I/^{99m}Tc$ (2, 8, 12, 16), $^{131}I/^{111}In$ and $^{111}In/^{113m}In$ (13), $^{111}In/^{99m}Tc$ (17, 18), and ^{99m}Tc in combinations including 2 or 3 tracers (19–22). Subtraction technique has significantly enhanced detections of labeled antibodies in tumors and infection foci in experimental studies (23–25).

The aim of the present study was to analyze two ^{99m}Tc-labeled compounds with different behavior in liver, estimate detection limits for liver lesions, and evaluate subtraction as an enhancement method for liver metastasis detection. In order to simulate the patient measurements liver phantom containing hot and cold areas of different sizes was constructed. The aim was to find out detection limits for activity concentration in lesions with varying size surrounded by constant liver and body activity levels.

Materials and Methods

Patients. Thirty-two patients with histologically confirmed cancer were included into the study; 27 patients had breast cancer and 5 lung cancer. Selection criteria and other characteristics are described elsewhere (19, 21). Thirteen of these patients had liver metastases (CT, US) and only four patients had clearly observable abnormal liver uptakes in planar MoAb images.

Radioantibody. The monoclonal antibody (BW 431/26) was provided by Behringwerke (Marburg, FRG). This IgG_1-subclass antibody was labeled with ^{99m}Tc using a stannous reduction technique (19). The labeling efficiency was always over 98%, and the immunoreactivity 80–85%, as tested by the manufacturer.

Imaging protocol. All the patients were imaged at least twice. The whole body was scanned at 3–5 h and 20–24 h after injection both with planar spot images and whole body images after single intravenous injection of ^{99m}Tc-labeled antibody. The radioantibody activity was 925–1110 MBq per 2 mg of labeled antibody, which was injected in 5 ml of physiological saline after informed consent from the patient. The imaging device was General Electric 500 Maxi gamma camera (General Electric Corp., Milwaukee, Wisc., USA) equipped with a low energy general purpose collimator. The gamma camera was combined with Star data processing system (Nova computer). For each scintigram at 3–5 h 1.2 megacounts (Mcts) and a 20–24 h 0.7 Mcts were collected using matrix size 128 × 128. The whole body scanning speed was 10 cm/min. The resolution at 15 cm distance from the face of the collimator was about 10 mm (FWHM). The energy resolution for 140 keV is 9% (FWHM). The intrinsic resolution of the gamma camera in bar-phantom air measurements using general purpose collimator is 2 mm.

Pharmacokinetics and biodistribution of the MoAb. The serum activity of the radioantibody was measured by taking samples just before, and consecutively up to 25 h after the injection. The disappearance rate of the radiolabeled antibody was measured from the blood samples of the three patients. The exponential function

$$A = A_0 e^{-kt} \quad [1]$$

was fitted using the iteration technique. The biological half-life of the antibody in the blood circulation could be calculated and its value was 23.3 h. The corresponding effective half-life was 4.7 h. The percentual activity distribution in different organs was calculated using regions of interest (ROI)-technique by drawing ROIs around organs in AP and PA views for conjugate view counting method (26). This method takes into account the counts observed from both directions (AP, PA), the geometric mean, and attenuation correction. The calculated counts in 4 and 24 h-images were corrected with the physical half-life of ^{99m}Tc. The biodistributions of radioactivity in various organs at 4 and 24 h were calculated using ROI-technique: the counts in various organs were measured as relative ratios compared with the whole body counts. The estimated liver activities were thus $6.1 \pm 0.8\%$ of injected activity at 4 h and $4.6 \pm 0.9\%$ at 20–24 h.

Subtraction imaging. During the last imaging phase (20–24 h) liver subtraction studies were performed in all these patients. The patient was first injected with ^{99m}Tc-labeled phytate (Solco-Phytate, Solco Ltd., Basle, Switzerland). The activity was 52–81 MBq and the imaging started 3–5 min after the injection. The patient was lying supine in the same position during all imaging procedures. The whole procedure took 10–15 min and no artefacts related to movement were observed.

Subtraction calculations. From the antibody image (I_a), the liver image (I_l) was subtracted pixel by pixel using a manually encircled region of interest (ROI) around the liver. N_1 is the number of counts per pixel in the antibody image and t_1 is the corresponding imaging time. The liver image, with ^{99m}Tc-phytate was made immediately after antibody imaging. If the number of counts per pixel in the liver image is N_2 and the imaging time t_2, then the count rates are N_1/T_1 and N_2/t_2 respectively. If we collect the same total number of counts per pixel in both images, then $N_1 = N_2$. Since the liver image contains counts/pixel from the antibody image, the imaging time t_1 is always $> t_2$. The corrected count rate in the liver is $N_1/t_2 - N_1/t_1 = N_1(t_1 - t_2)/(t_1 t_2)$ and the number of counts per pixel in the liver is $N_1(t_1 - t_2)/t_1$. Now we can easily subtract the corrected liver image from the antibody image (I_a) and construct the subtraction image (I_s) using the following equation

$$I_s = I_a - k \times N_1(t_1 - t_2)/t_1, \quad [2]$$

where k is the scaling factor. This equation presents the real liver colloid image, corrected by this time factor. The

real subtracted image (MoAb-image-corrected colloid-image) is then obtained using scaling factors iteratively, so that the liver background approaches zero (on digital subtraction images). Since the subtraction images are made only from AP-direction (24 h antibody image) and the colloid activity is much higher than the activity in the antibody image, this kind of approximation is possible. The iteratively obtained scaling factor k multiplies the counts in each pixel yielding visually good subtraction results.

Phantom measurements. In order to simulate the patient subtraction studies a liver phantom was constructed, containing hot and cold areas of different sizes representing lesions (Fig. 1). The hot lesions filled with ^{99m}Tc-solution were 5, 10 and 20 min in diameter (∅) and 20 mm deep. These small cylinders served as cold lesions when no radioactive water was present and their volumes were 0.33, 1.33, and 5.34 ml respectively. The cold plastic lesions (∅ 27–32 mm) had 5, 10 and 15 mm deep holes with 10 mm in diameter, and they were connected through small capillaries with the surrounding liver compartment with a volume of 0.35 l. Thus, the activity distribution was equal to surrounding liver activity. These plastic buttons corresponded to nearby cold areas on gamma images and were used as reference ROI areas for subtraction calculations. The specific activity in hot lesions varied from 1.85 to 14.8 MBq/ml corresponding to activities in patient studies. The cold lesions were filled with non-radioactive water. The 3 cm thick phantom was placed in an elliptic cylindrical container, 20 cm thick and with 9.0 l volume, corresponding to the cross section of adult abdominal body. The liver phantom was situated at a depth of about 10 cm from both anterior and posterior directions, when imaged by the gamma camera. The activities of radioactive water in the liver phantom and the body cylinder were chosen to give about 10% and 3% of the total count rates in planar imaging and kept constant during the measurements. A point source outside the liver phantom but inside the body phantom acted as standard, and all the count rates were corrected for ^{99m}Tc-decay. This phantom was imaged from AP and PA directions in planar mode with 5 Mcts each with a Picker DDC gamma camera equipped with Gamma-11 software. ROIs were delineated and summed up from the two projections using the conjugate view counting method. Count rates were corrected for the total imaging time of each frame and for ^{99m}Tc decay. The count rates in hot lesions were subtracted by normal liver count rates and void ROI values respectively (representing cold metastases) were subtracted from hot lesion values. Subtraction was performed so that count rates within reference ROI areas approached zero, corresponding to a liver background zero activity in the clinical situation.

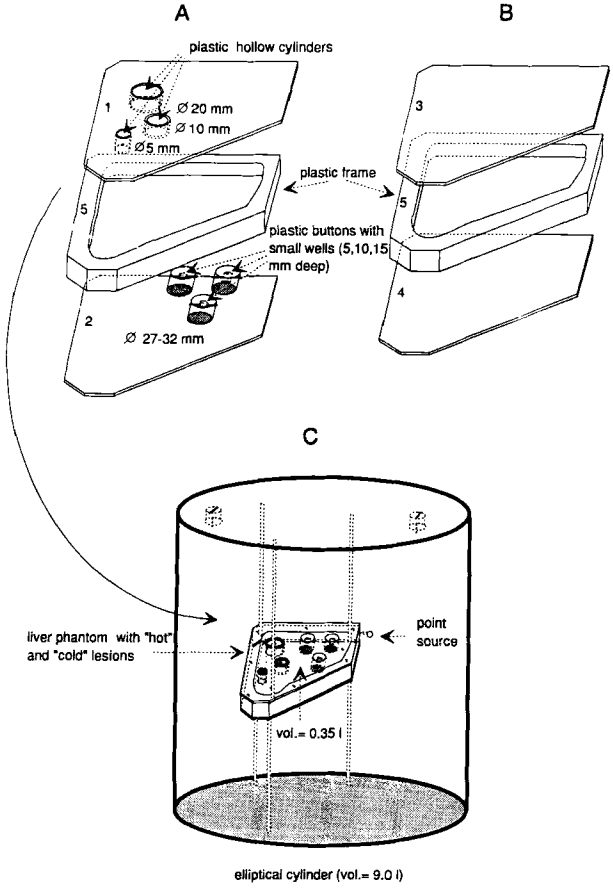

Fig. 1. Schematic illustration of the liver phantom construction inside the body phantom (C). the liver phantom contains hot and cold lesions with the setting 1 + 5 + 2 (A), and normal liver with the combination 3 + 4 + 5 (B). A and B combinations were used in the present study.

Results

The patient measurements and the following image evaluation included three phases (19, 21, 22): 1) Imaging of liver at 24 h after the injection of 1 000 MBq ^{99m}Tc-labeled anti-CEA MoAb; 2) Liver imaging with 75 MBq ^{99m}Tc-phytate (metastases usually visualized as defects) at 24 h; 3) Subtraction of the phytate + MoAb image from the original antibody image.

The criterion used for proper subtraction was to obtain the best possible cancellation of normal liver activity according to equation [2]. Fig. 2 demonstrates a patient study where all these images are included, i.e., the originally recorded ^{99m}Tc-MoAb-image (A), the originally recorded ^{99m}Tc-MoAb + ^{99m}Tc-colloid-image (B), the corrected ^{99m}Tc-colloid-image (C), the subtracted ^{99m}Tc-MoAb – ^{99m}Tc-colloid-image (D). The (C) image was obtained by subtracting (A) and (B), using equation [2]. The (D) image finally, was obtained by subtracting (C) and (A) using the best possible cancellation of normal liver activity by iterating with scaling factors.

Residual activity after subtractions was obtained in 14 patients. Two false positive findings were observed, and

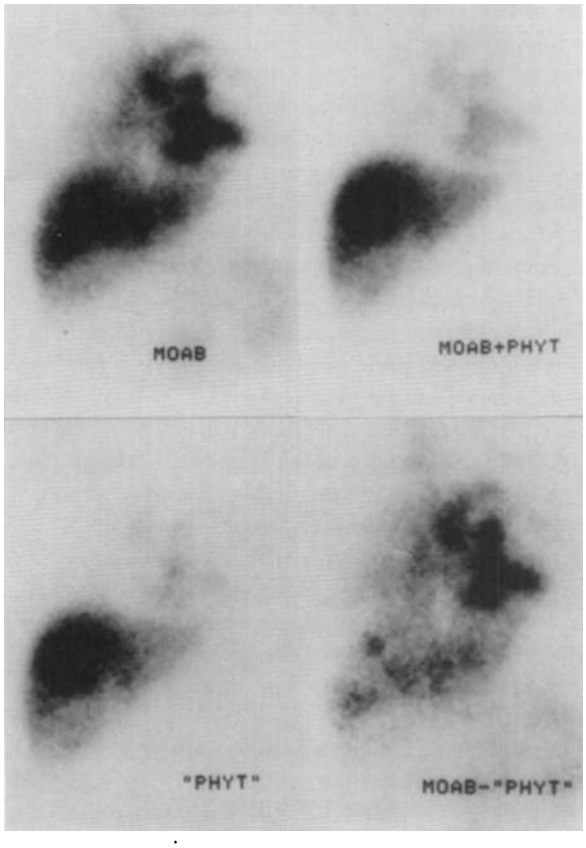

Fig. 2. A patient study with originally recorded ^{99m}Tc-MoAb-image (A), originally recorded ^{99m}Tc-MoAb + ^{99m}Tc-colloid image (B), corrected ^{99m}Tc-colloid image (C), subtracted ^{99m}Tc-MoAb $-^{99m}$Tc-colloid image (D). (C) image was by subtracting (A) from (B) using time correction as explained in the text. Finally the (D) image was obtained by subtracting (C) from (A) using iteration for liver background activity (equations [2]).

two false negative findings as compared to conventional diagnostic methods (CT, US). Thirteen patients had liver metastases; the detection rate was 11/13 and the specificity 17/19. Planar ^{99m}Tc-MoAb showed positive uptakes in only four patients, whereas planar ^{99m}Tc-colloid images showed defects in 12 patients.

In the phantom studies count rates in hot lesions were subtracted by the average liver count rates and respectively void ROI values were subtracted from hot lesion ROI values and by corresponding voids (representing cold metastases) in the liver phantom. In Fig. 3, three examples of various specific activities are presented in a phantom study. On the left are the images with radioactive water, in the middle the corresponding images with non-radioactive water, and on the right the subtracted images. The images show that in this geometry lesions of size 1.3 cm^3 can be detected when the signal-to-background ratio is larger than 1.2 (see also Fig. 4). The subtraction (hot lesions $-$cold lesions) shows that this ratio needs to be only 1.1 when the specific activity in a lesion is 1.85 kBq/ml and in liver itself 1.0 MBq/ml. In conclusion, the ratio of specific activity in lesion to that of adjacent liver had to be larger than 1.7, 2.4 and 3.5 when the lesions had the volumes 5.3, 1.3, and 0.3 cm^3 respectively. In all these experiments the depth of the cylindrical hot lesion was 20 mm and it was situated at a depth of 10 cm in the water phantom; the specific activity of the liver was 1.0 MBq/ml.

Fig. 4 gives tumor-to-normal liver ratio as the function of specific activity of the hot lesions in MBq/ml, corresponding to phantom studies like the one in Fig. 3. Fig. 5 demonstrates how the subtraction enhances the lesion detectability, in conditions when the lesion is situated in the middle of the abdomen, inside liver. As a function of specific activity and lesion size, the subtraction is performed vs holes and normal liver. This shows that lesions larger than 5 mm in diameter (volume 0.33 ml) can be detected. Fig. 5 demonstrates the worst case (when the lesion is in the middle of the abdomen), and the detectable lesion ratios for MAB-FYTATE subtraction and MAB-liver subtraction are 1.5 and 1.1, (lesion size 5.3 ml) and 1.3 and 1.1 (lesion size 1.3 ml). In these cases the subtraction gives additional information by a factor 4 $(1.4 - 1.1/(1.1 - 1.0))$ and a factor 2 $(1.3 - 1.1/(1.1 - 1.0))$. In the best cases, when the lesion was close to the phantom surface, this subtraction method gave additional information with a factor 2 when the lesion size was 0.3 cm^3, and with a factor 9 when the size was 5.3 cm^3 and the specific activity in the lesion was at least twice as high as in adjacent liver. The smallest lesions could not be detected under any circumstances in the middle of liver. This would mean that when injecting 1.11 MBq ^{99m}Tc-labeled antibody, a level of approximately 0.02% (ID) in g in a liver metastasis has to be achieved before this subtraction technique gives additional information.

Discussion

Thirteen patients had liver metastases (CT, US), and only four patients clearly observable abnormal liver uptakes in planar MoAb images. In 9 cases additional information concerning liver metastases with subtraction technique was obtained, and on the basis of our phantom measurements the enhanced detectability was not an artefact. However, the enhanced detectability of liver metastases in our study was largely depending on the superiority of phytate imaging for liver scanning. In our study the detection rate was about 90%, which is concordance with our studies (27).

SPECT increases significantly the role of antibody imaging for detection of liver metastases (28, 29), and should be used even routinely for liver studies. The findings should preferably be compared with the corresponding CT scans and, even better, may be obtained by fusion analysis of the CT and SPECT images (30).

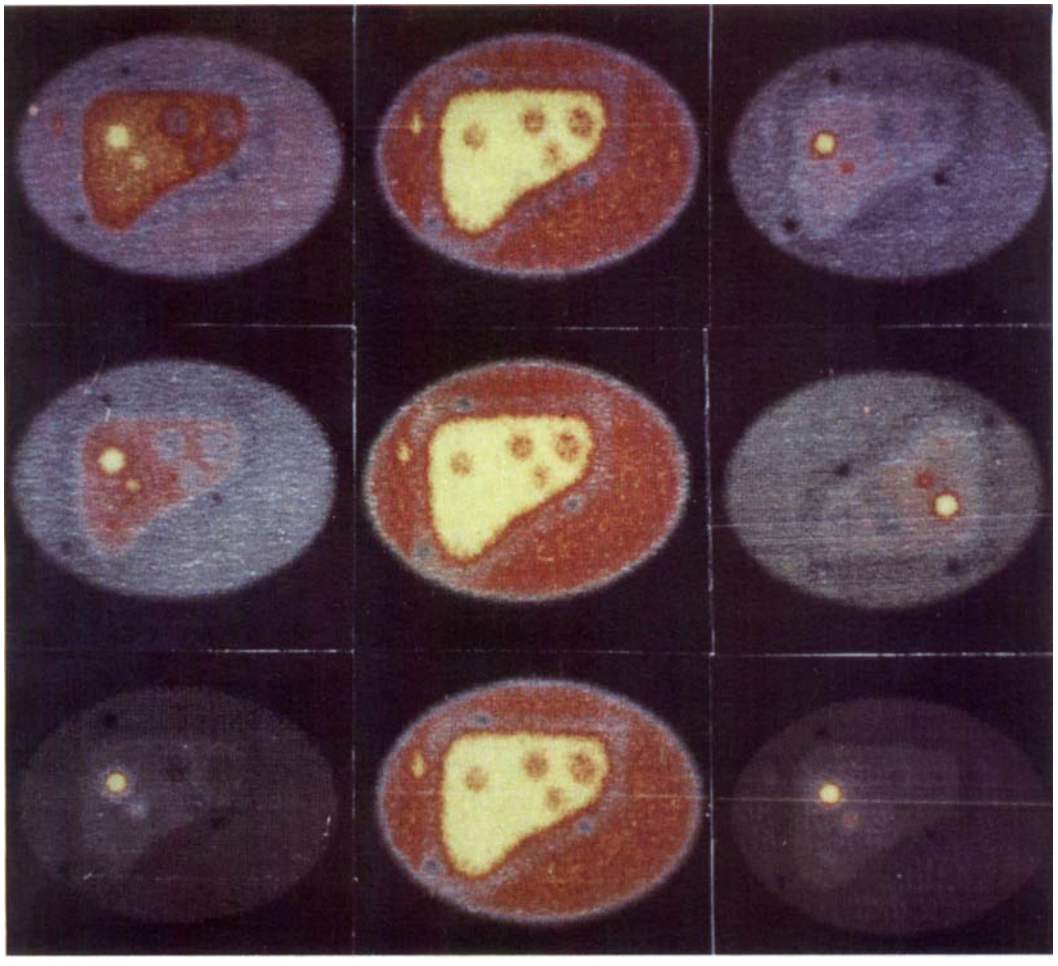

Fig. 3. A phantom study: three examples of various specific activities are presented, with the liver phantom in the middle of the body phantom. On the left there are images with radioactive water (with decreasing normal liver activity from top to bottom), in the middle the corresponding images with non-radioactive water, and on the right the subtracted images. In the subtracted images the counts in the reference ROI areas approached zero. The specific activities in the lesions were 12.8, 7.4, 2.8 MBq/ml, and in the surrounding liver 1.0 MBq/ml.

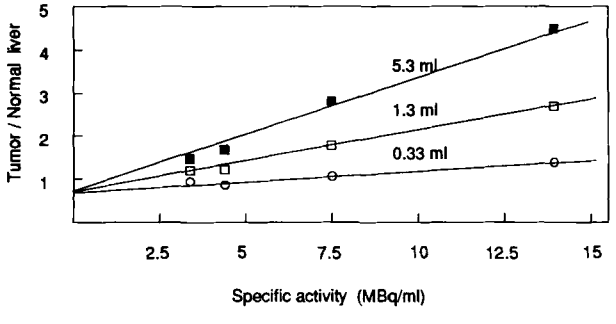

Fig. 4. Lesion-to-normal liver ratios (absolute counts/pixel/ROI/conjugate view (26)) as the function of specific activity of the hot lesions in MBq/ml. The tumors are situated in the middle of the liver (worst possible case). The lines represent different volumes of hot lesions. The visual detection limit on gamma image was approximately 1.2.

However, our patients, had multiple lesions and were studied by whole-body scanning; the subtraction was a quick and handy procedure performed at the end of long imaging study.

Both primary cancers and metastatic neoplasms in the liver have sometimes a diffuse growth without well-defined borders to the surrounding parenchyma. This is contrary to phantom measurements, where distinct borders are usually constructed, whereas mimicry of diffuse lesions would require a special design. However, the specific activity in lesion and surrounding tissues (and therefore tumor-to-non-tumor ratio) is a parameter, which can be measured both in phantom and in patient imaging. Another difference between phantom and patient imaging is the much better statistical certainty, obtainable in phantom measurements, e.g., when 10 Mcts are collected against about 0.7–1.2 Mcts in patient imaging. The standard deviation values for the liver region in a 128×128 image matrix mode are therefore in the range of 1 and 5% respectively.

A double-headed gamma camera was not available for our patient subtraction procedure and therefore subtraction calculations were performed with AP view data only according to equation [2]. The detection limits in phantom measurements were calculated using the conjugate view

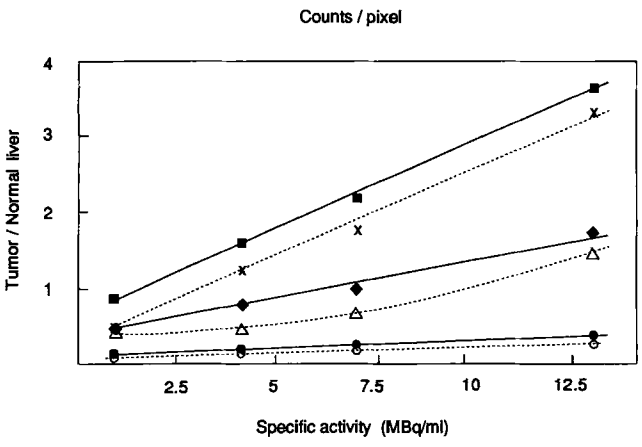

Fig. 5. The subtraction enhances the lesion detectability, in conditions where the lesion is situated inside the liver in the middle of the abdomen as function of specific activity; subtraction (hot lesions (MAB) – voids (FYTATE) vs subtraction (hot lesions (MAB) – normal liver (FYTATE)). The calculations are based on absolute counts/pixel in corresponding ROIs using the conjugate view method (26).
MAB – FYTATE: ■ 5.3 ml; ◆ 1.3 ml; ● 0.3 ml
MAB – liver: × 5.3 ml; △ 1.3 ml; ○ 0.3 ml

method which gives better statistical information. We also studied phantom measurements entirely from AP view. The detection limits, as presented in our study, were very similar for conjugate view and single AP view; naturally, the statistics was better for conjugate view and the presented results are therefore more reliable. Patient geometry and size also influence the results. Firstly, increased absorption in tissues as a function of depth reduces the number of counts and the statistical certainty. Secondly, increased distance from the gamma camera enlarges the view of collimator holes decreasing the resolution and thus the minimum size of a detectable lesion.

Scattered radiation is an important constrast decreasing factor in nuclear medicine imaging. However, we have not specifically tackled this problem in the present study, since it similarly affects both phantom and patient examinations. Scattered radiation accounts for up to 25% of the signal in ^{99m}Tc-scanning. In the present study this turned out not to be impertinent for the images, because no halo signs around the lesions were observed. The subtraction of hot and cold lesions has, however, a tendency to decrease the negative effects of scattering, although it inevitably increases the background noise.

From the phantom measurements we conclude that lesions larger than 5 mm in diameter in the middle of a 20 cm thick body phantom can be detected by a combined AP and PA imaging mode. Subtraction gave additional information by a factor 2–9, when the lesion size varied from 0.3 to 5.3 cm^3 and when the specific activity in the lesion was at least twice as high as in adjacent liver.

REFERENCES

1. Larson SM. Cancer imaging with monoclonal antibodies. In: Devita VT. Jr, Hellman S, Rosenberg SA, eds. Important advances in oncology 1986. J. P. Lippincott Co. 1986; 233–49.
2. Goldenberg DM, Goldenberg H, Sharkey RM, et al. Imaging of colorectal carcinoma with radiolabeled antibodies. Semin Nucl Med 1989; 19: 262–81.
3. Halpern SE, Dillman RO. Review. Problems associated with radioimmunodetection and possibilities for future solutions. J Biol Resp Modif 1987; 6: 235–62.
4. Epenetos AA, Snook D, Durbin H, Johnson PM, Taylor-Papadimitriou J. Limitations of radiolabeled monoclonal antibodies for localization of human neoplasms. Cancer Res 1986; 46: 3183–91.
5. Goldenberg DM Sharkey RM, Ford E. Anti-antibody enhancement of iodine-131 anti-CEA radioimmunodetection in experimental and clinical studies. J Nucl Med 1987; 28: 1604–10.
6. Sands H. Experimental studies of radioimmunodetection—Overview. Cancer Res 1990; 50: 809s–13s.
7. Pimm MV, Fells HF, Perkins AC, Baldwin RW. Iodine-131 and indium-111 labelled avidin and streptavidin for pretargetted immunoscintigraphy with biotinylated anti-tumour monoclonal antibody. Nucl Med Commun 1988; 9: 931–41.
8. Green AJ, Begent RHJ, Keep PA, Bagshawe KD. Analysis of radioimmunodetection of tumors by the subtraction technique. J Nucl Med 1984; 25: 96–100.
9. Nimmon CC, Carroll MJ, Flatmann W, et al. Spatial probability mapping of change: application to gamma camera quality control and immunoscintigraphy. Nucl Med Commun 1984; 5: 231–4.
10. Tuscan MJ, Wahl RL, Botti J. Dynamic graded subtraction: a simple method to background correct and display multicompartmental radiopharmaceutical scintigrams. J Nucl Med Tech 1985; 13: 121–4.
11. Fairweather DS, Irwin M, Bradwell AR, Dykes PW, Flinn RM. Computer analysis on antibody scans. Protides Biol Fluids 1983; 31: 285–8.
12. Chandler ST, Anderson P. A method for thresholding subtracted images in radiolabelled-antibody imaging. Br J Radiol 1987; 60: 881–6.
13. Liehn JC, Hannequin P, Nasca S, Lebrun D, Cattan A, Valeyre J. A new approach to image subtraction in immunoscintigraphy: preliminary results. Eur J Nucl Med 1987; 13: 391–6.
14. Perkins AC, Whalley DR, Hardy JG. Physical approach for the detection of dual radionuclide image subtraction artefacts in immunoscintigraphy. Nucl Med Commun 1984; 5: 501–12.
15. Marymont JH, McKenzie MB, McKay M. An experimental model for evaluation of dual isotope subtraction techniques. J Nucl Med Tech 1987; 15: 119–20.
16. North WG, Hirsh V, Lisbona R, Schultz J, Cooper B. Imaging of small cell carcinoma using ^{131}I-labelled antibodies to vasopressin associated human neurophysin (VP-HNP). Nucl Med Commun 1989; 10: 643–52.
17. Kairemo KJA, Lehtovirta P. Radioimmunodetection of uterine leiomyosarcoma with ^{111}In-labeled monoclonal antimyosin antibody Fab fragments. Gynecol Oncol 1990; 36: 417–22.
18. Chetanneau A, Lehur PA, Ripoche D, et al. Histological correlation of 17 prospective immunoscintigraphies of recurrences of colorectal carcinomas using indium-111-labeled anti-CEA and(or) Ca 19-9 monoclonal antibodies. Eur J Nucl Med 1989; 15: 302–6.

19. Kairemo KJA. Immunolymphoscintigraphy with Tc-99m labeled monoclonal antibody (BW 431/26) reacting with carcinoembryonic antigen in breast cancer. Cancer Res 1990; 50: 949S–54S.
20. Ruther W, Hotze A, Moller F, Bockisch A, Heitzman P, Biersack HJ. Diagnosis of bone and joint infection by leucocyte scintigraphy. A comparative study with ^{99m}Tc-HMPAO-labelled leucocytes, ^{99m}Tc-labelled antiganulocyte antibodies and ^{99m}Tc-labelled nanocolloid. Arch Orthop Trauma Surg 1990; 110: 26–32.
21. Aronen HJ, Paavonen T, Heikkonen J, et al. Imaging of non-small cell lung cancer with ^{99m}Tc-labeled monoclonal anti-CEA antibody with a comparison to immunohistochemistry. Antibody Immunoconj Radiopharm 1991; 4: 569–75.
22. Kairemo KJA, Kiuru AA, Heikkonen JJ. ^{99m}Tc-MoAb and ^{99m}Tc-colloid image subtraction analysis in evaluation of liver lesions; phantom measurements and clinical studies. J Nucl Med 1992; 33: 913.
23. Collet B, Pellen P, Marti A, Moisan A, Bourel D, Toujas L. Scintigraphic detection in mice of inflammatory lesions and tumours by an indium-labelled monoclonal antibody directed against Mac-1 antigen. Cancer Immunol Immunother 1988; 26: 237–42.
24. Longley C, Furmanski P, Dienhart DG, et al. Pharmacokinetics, biodistribution, and gamma camera imaging of ^{111}In-KC-4G3 murine monoclonal antibody in athymic nude mice with or without human tumor xenografts. Cancer Res 1990; 50: 5954–61.
25. Beyers M, Aspinall S, Conradie JD, Fourie PJ. Radioiodination of murine anti-alpha-foetoprotein E.9 monoclonal antibody and its F(ab)$'_2$ fragment for the diagnosis of hepatocellular carcinoma. Nuklearmedizin 1988; 27: 87–94.
26. Thomas SR, Maxon HR, Kereiakes JG. Techniques for quantitation of in vivo radioactivity. In: Gelfand MJ, Thomas SR, eds. Effective use of computers in nuclear medicine. New York: McGraw Hill, 1988: 468–84.
27. Mochizuki T, Takechi T, Murase K, Shigesawa, Watanabe Y, Hamamoto K. Liver tumor imaging by thallium-201 and technetium-99m phytate with high resolution three head SPECT. J Nucl Med 1992; 33: 918.
28. Happ J, Baum RP, Frohn J, et al. Immunszintigraphie mit ^{111}In-DTPA-markierten monoklonalen Antikörpern: Vergleich zwischen ECT und planarer Szintigraphie. Nucl Med 1987; 26: 258–62.
29. Lind P, Lechner P, Arian-Schad K, et al. Anti-carcinoembryonic antigen immunoscintigraphy (technetium 99m-monoclonal antibody BW 431/26) and serum CEA levels in patients with suspected primary and recurrent colorectal carcinoma. J Nucl Med 1991; 32: 1319–25.
30. Kramer EL, Noz ME. CT-SPECT fusion for analysis of radiolabeled antibodies: applications in gastrointestinal and lung carcinoma. Int J Rad Appl Instrum [B] 1991; 18: 27–42.